Japan Antibiotics
Research Association

The Society for
Actinomycetes Japan

ARTICLE

Identification of novel small-molecular inhibitors of *Staphylococcus aureus* sortase A using hybrid virtual screening

Galyna P. Volynets[1] · Fabian Barthels[2] · Stefan J. Hammerschmidt[2] · Olena V. Moshynets [3] · Sergiy S. Lukashov[1] · Sergiy A. Starosyla[1,4] · Hanna V. Vyshniakova[5] · Olga S. Iungin[6] · Volodymyr G. Bdzhola [1] · Andrii O. Prykhod'ko[1,7] · Anatolii R. Syniugin[1] · Vladislav M. Sapelkin[1] · Sergiy M. Yarmoluk[1] · Tanja Schirmeister[2]

Abstract

Staphylococcus aureus is one of the most dangerous pathogens commonly associated with high levels of morbidity and mortality. Sortase A is considered as a promising molecular target for the development of antistaphylococcal agents. Using hybrid virtual screening approach and FRET analysis, we have identified five compounds able to decrease the activity of sortase A by more than 50% at the concentration of 200 μM. The most promising compound was 2-(2-amino-3-chloro-benzoylamino)-benzoic acid which was able to inhibit *S. aureus* sortase A at the IC_{50} value of 59.7 μM. This compound was selective toward sortase A compared to other four cysteine proteases – cathepsin L, cathepsin B, rhodesain, and the SARS-CoV2 main protease. Microscale thermophoresis experiments confirmed that this compound bound sortase A with K_D value of 189 μM. Antibacterial and antibiofilm assays also confirmed high specificity of the hit compound against two standard and three wild-type, *S. aureus* hospital infection isolates. The effect of the compound on biofilms produced by two *S. aureus* ATCC strains was also observed suggesting that the compound reduced biofilm formation by changing the biofilm structure and thickness.

✉ Galyna P. Volynets
  g.p.volynets@gmail.com

1 Department of Medicinal Chemistry, Institute of Molecular Biology and Genetics, the NAS of Ukraine, 150 Zabolotnogo St, 03143 Kyiv, Ukraine

2 Institute of Pharmaceutical and Biomedical Sciences, Johannes Gutenberg-University of Mainz, Staudinger Weg 5, 55128 Mainz, Germany

3 Biofilm study group, Institute of Molecular Biology and Genetics, the NAS of Ukraine, 150 Zabolotnogo St, 03143 Kyiv, Ukraine

4 RECEPTOR.AI, Boston, MA, USA

5 L.V. Gromashevsky Institute of Epidemiology and Infectious Diseases NAMS of Ukraine, 5 Amosova St, 03038 Kyiv, Ukraine

6 Department of Functional Genomics, Institute of Molecular Biology and Genetics, the NAS of Ukraine, 150 Zabolotnogo St, 03143 Kyiv, Ukraine

7 Research and Development Department, Scientific Services Company Otava Ltd, 150 Zabolotnogo St, 03143 Kyiv, Ukraine

Introduction

Staphylococcus aureus (*S. aureus*) is one of the most common nosocomial pathogens that causes a number of hospital-acquired diseases ranging from skin infections to severe human infections associated with high levels of morbidity and mortality such as sepsis, endocarditis, osteomyelitis, necrotizing pneumonia, etc [1–3].

The main problem of staphylococcal infections treatment is the increasing emergence of multidrug resistance. Nowadays, methicillin- (MRSA) and vancomycin-resistant *S. aureus* (VISA and VRSA) strains remain serious medical and public problems worldwide since the antibiotics of the last choice such as linezolid, teicoplanin and daptomycin are not always effective and have shown a tendency to lose their effectiveness due to resistance [4–8]. Therefore, the development of novel types of antistaphylococcal agents is of great importance.

Sortase A is recognized as a promising druggable anti-virulence target [9–12]. Sortase A is a membrane-localized cysteine transpeptidase that catalyzes the attachment of surface virulence proteins to the cell wall [13], which play essential roles in infection processes by promoting bacterial

adhesion, biofilm formation, host cell entry, acquisition of important nutrients from the host, immune evasion and suppression [14, 15]. Sortase A is a promising target since it is localized on the extracellular side of the cell membrane. This enhances the bioavailability of the inhibitor due to accessibility of the target with no requirement for penetration through the bacterial cell wall. Another advantage is that the sortase A does not have human homologs hence selective inhibitors of this enzyme should possess lower toxicity. Sortase A is not crucial for bacterial growth and viability, and therefore, the inhibition of this enzyme is expected to cause lower selection pressure on resistance development [15, 16].

To date, several chemical classes of sortase A inhibitors have been reported among synthetic and natural compounds, [12, 16–21] but none of them have entered clinical trials as yet. Therefore, it is of great interest for medicinal chemistry to discover novel chemical scaffolds of sortase A inhibitors.

Materials and methods

Molecular docking

The semi-flexible receptor-ligand docking was performed with the DOCK package [22–25]. As a receptor, the crystal structure of *S. aureus* sortase A with PDB accession code:2MLM was used [26]. The ligands geometry was calculated with YFF force field [27] and the partial atomic charges were added using the Kirchhoff method [28]. Docking parameters were set as reported previously [29]. The spheres in the active site of SrtA were generated with the DOCK *sphgen* program. Grid maps were built using the *grid* program with grid spacing 0.3 Å. The all-atom model was used for protein representation. We selected "multiple anchor" parameter for molecular docking and the minimal number of atoms in the achor was 6 and the maximum number of orientations was 1000.

Visual analysis of docking complexes was carried out with Discovery Studio Visualizer 4.0 [30].

Pharmacophore modeling

Receptor-oriented pharmacophore models were generated based on the two crystal structures of *S. aureus* SrtA with the ligands. The first primary pharmacophore model was built taking into account the intermolecular bonds of the small-molecular inhibitor benzo[d]isothiazol-3-one with SrtA (PDB ID: 2MLM) [26] and the second pharmacophore model was developed based on the complex of polypeptide substrate with SrtA (PDB ID: 2KID) [31]. The excluded volumes were generated using the atoms of amino acid residues in the active site of SrtA within 5 Å of the ligand.

These models were optimized in different ways: excluding several pharmacophore features, changing the radii, and scores of pharmacophore features. Therefore, a number of derivative pharmacophore models were obtained. Pharmacophore model validation was performed by screening towards a training set containing 173 known inhibitors of SrtA (cutoff of activity was 30 μM). As a result, nine pharmacophore models, which correctly predicted active and inactive compounds from the training set, were selected for pharmacophore screenings of the OTAVA compound collection [32].

Sortase A (SrtA) expression and purification

Expression of the *S. aureus* SrtA was mainly performed as described previously [33]. The SrtA-sequence containing pET23b expression construct was transformed into competent cells of the *Escherichia coli* (*E. coli*) strain BL21-Gold (DE3) (Agilent Technologies, Santa Clara, California) and grown in 100 μM ampicillin containing LB medium at 37 °C until they reached an OD_{600} of ~0.6–0.8. Expression was induced with addition of 1 mM isopropyl-D-thiogalactoside (IPTG) for 16 h at 20 °C. After harvesting by centrifugation (10 min, 10 krpm), cells were resuspended in lysis buffer (20 mM Tris, pH 6.9, 300 mM NaCl, 0.1% (v/v) $Triton_{X-100}$, DNase, lysozyme) and lysed by sonication (Sonoplus, Bandelin, Berlin, Germany). The cleared lysate (45 min, 15 krpm) was subjected to IMAC (HisTrap HP 5 ml column, GE Healthcare, Chicago, Illinois) to crudely isolate the protein. Eluted fractions containing protein were subsequently administered to a gel-filtration (size exclusion chromatography, SEC) step (HiLoad 16/60 Superdex 75 column, GE Healthcare) in the SEC/storage buffer (20 mM Tris-HCl, pH 7.5, 150 mM NaCl, 5 mM $CaCl_2$). Purified SrtA was shock frozen in liquid nitrogen and stored at −80 °C until further use. Throughout all steps, protein concentrations were measured via absorbance at 280 nm and sample purity was assessed via SDS-PAGE.

In vitro Sortase A inhibition assay

Assays of *S. aureus* SrtA transpeptidation activity were performed as previously described [12]. Briefly, recombinantly expressed SrtA (final concentration: 1 μM) was incubated in assay buffer (50 mM Tris, 150 mM NaCl, 5 mM $CaCl_2$, pH 7.5) with 25 μM of Abz-LPETG-Dap(Dnp)-OH and 0.5 mM H_2N-(Gly)$_4$-OH. Inhibitors were added from DMSO stocks. Assays were initiated by the addition of SrtA and monitored for 30 min at 30 °C in an Infinite M200 Pro plate reader with λ_{ex} 320 nm/λ_{em} 430 nm. Three technical replicates were performed for each inhibitor in flat-bottomed black 96-well plates. Enzyme inhibition was analyzed as previously described [12].

Protease inhibition selectivity

Fluorometric assays for cathepsin B, cathepsin L, and rhodesain were performed as described previously [12]. Cbz-Phe-Arg-AMC was used as the fluorogenic substrate (100 µM for cathepsin B, 6.5 µM for cathepsin L, and 10 µM for rhodesain). Fluorometric assays for SARS-CoV2 M^{pro} were performed as described previously [34]. Dabcyl-KTSAVLQSGFRKME-Edans was used as a FRET-substrate at a final concentration of 20 µM.

Microscale thermophoresis

Purified *S. aureus* sortase A was labeled with the Monolith Protein Labeling Kit RED-NHS according to the manufacturer's instructions. MST sample preparation was conducted as described by the manufacturer's standard protocols. Briefly, MST reaction mixtures consisted of 5 nM labeled sortase A in MST buffer (50 mM Tris, 150 mM NaCl, 5 mM CaCl$_2$, 0.05% (v/v) Tween-20, 10% DMSO, pH 7.50) supplemented with a 1:1 dilution series of the hit compounds (500-31 µM). MST measurements were performed with a NanoTemper Monolith NT.115 instrument (MST power of 50%, LED power of 70%, 20 s laser-on time, and 5 s laser-off time) with NanoTemper Monolith premium capillaries. Binding affinities (K$_D$) were determined with the Nanotemper MO Analysis Software v2.3. Response evaluation was conducted at 10 s laser-on time.

Aggregation assessment by turbidimetry

To assess the aggregation potential of the identified hit compounds, a turbidimetric analysis was conducted. Therefore, the optical density (OD$_{610}$) was measured over time (assay buffer, no enzyme 200 µM compound concentration). Absorption measurements were conducted in 60 kinetic cycles of each 30 s with orbital shaking (300 rpm for 5 s before readout) using a Tecan Spark 10 M plate reader. Compounds did not show significant absorbance at this wavelength spectrum, thus, any increase in OD$_{610}$ was assumed to be caused by precipitation of the hit compound.

Strains and culturing conditions

S. aureus ATCC 25923, *S. aureus* ATCC 43300, *P. aeruginosa* PA 01, and *K. pneumoniae* ATCC 10031 (Ukrainian National Collection) were used as model strains for testing biofilm formation and free-living (planktonic) behavior under different concentrations of the tested compound. Biofilm responses to the compound were also determined for three *S. aureus* isolates from Ukrainian hospitals, including the multidrug (MDR) strains UHI 1, UHI 2, and UHI 3. The Kirby-Bauer disc-diffusion assay was used to determine the antimicrobial susceptibility of the *S. aureus* strains. Susceptibility was then determined as the diameter (mm) of inhibition or MIC value after incubation up two days and interpreted according to the European Committee on Antimicrobial Susceptibility Testing (EUCAST) guidelines [35] for the rest of the antibiotics.

Antibiotic susceptibility of the *S. aureus* strains listed in S2 Table. All strains were stored as frozen stocks in 25 (v/v) % glycerol at −80 °C.

Planktonic assay

Planktonic growth assays of *S. aureus* ATCC 25923, *S. aureus* ATCC 43300, *P. aeruginosa* PA 01, *K. pneumoniae* ATCC 10031 were assessed in loosely lidded 30 ml glass microcosms which were incubated with shaking before assay at 37 °C. The microcosms contained 5 ml Mueller-Hinton broth and the corresponding concentration of the tested compound or without. Aliquots of over-night culture were added to replicate vials ($n = 6$) to ~5×10^6 CFU ml^{-1} and growth was determined after 16 h incubation by removing 200 µl samples which were transferred to a polystyrene 96-well plate and OD620 measured using a Multiskan ™ FC Microplate Photometer (Thermo Fisher Scientific).

Biofilm assay

20 µl aliquots of over-night culture of *S. aureus* ATCC 25923, *S. aureus* ATCC 43300, *P. aeruginosa* PA01, *K. pneumoniae* ATCC 10031, and three UHI strains were used to inoculate replicate wells ($n = 5$ for each treatment) containing 200 µl Mueller-Hinton with the appropriate concentration of the tested compound or without. Growth (OD$_{620}$) was determined after 24–48 h static incubation at 37 °C using a Multiskan ™ FC Microplate Photometer (Thermo Fisher Scientific).
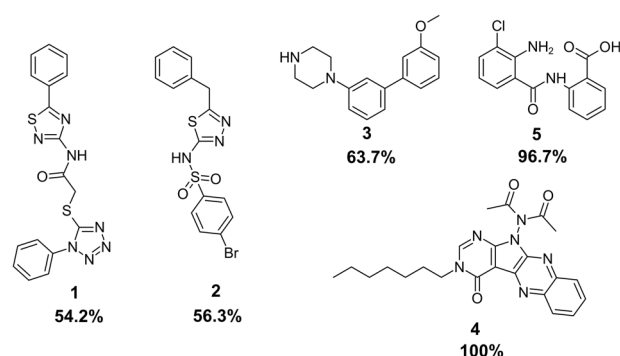

Fig. 1 Inhibitors of *S. aureus* sortase A. Chemical structure of hit compounds identified after screening at 200 µM inhibitor concentration and FRET-quenching correction

## Confocal laser scanning microscopy (CLSM)

Biofilm samples were prepared in 30 ml glass microcosms containing 5 ml Mueller-Hinton broth. The biofilm was stained with 1 mM ethidium bromide (Sigma) and 3 mM AmyGreen solution (own synthesis). No additional washing was used in order to limit the physical disruption of biofilm structures through liquid movement. The samples were not fixed, and a cover slip was placed over the stained samples before imaging. CLSM analysis was undertaken using a Leica TCS SPE Confocal system with coded DMi8 inverted microscope (Leica, Germany) and Leica Application Suite X (LAS X) Version 3.4.1. Images were acquired using excitation at 488 nm and emission collected at 490-580 nm for AmyGreen, and excitation at 532 nm and emission collected at 537-670 for ethidium bromide. The total pixels were calculated by the above-mentioned software.

Fig. 2 *S. aureus* sortase A pharmacophore models. Mapping of compound **1** (**a**) and compound **2** (**b**) to corresponding pharmacophore models. Pharmacophore features matched with generated models are labeled with green (H-bond acceptor), cyan (hydrophobic), and azure (aromatic feature without vector) color. Excluded volumes (labeled with gray color) were built on the atoms of amino acid residues in the active site of sortase A within 5 Å around the ligand
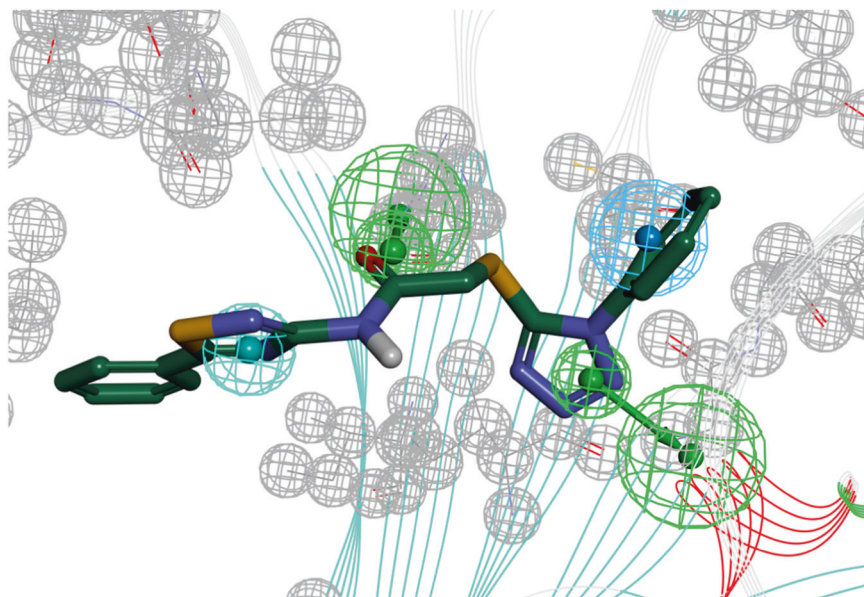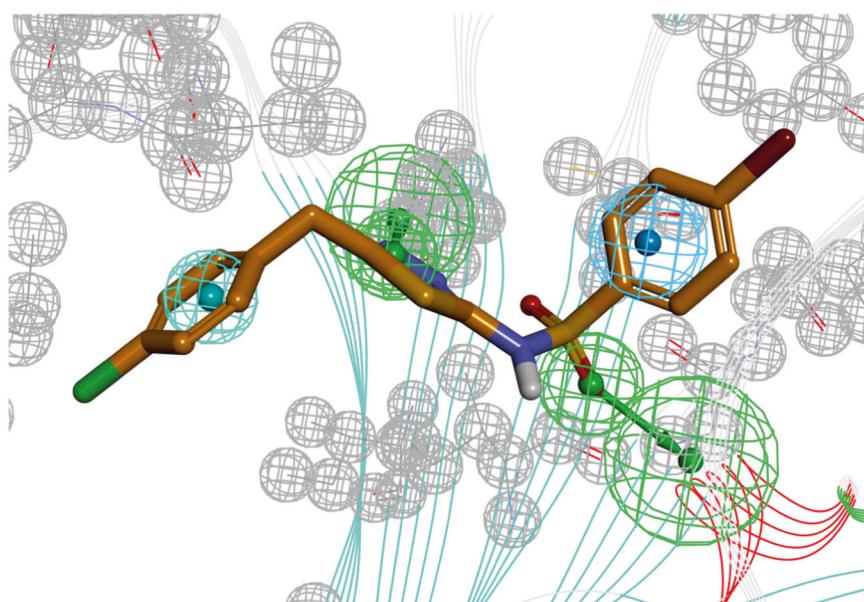
Fig. 3 The complexes of compounds **3** (**a**), **4** (**b**), and **5** (**c**) with amino acid residues in the active site of *S. aureus* sortase A, obtained with molecular docking. The hydrogen bonds are shown by green dashed lines, π-alkyl interactions are shown by yellow dashed lines, and π-cation interactions are indicated with orange dashed lines
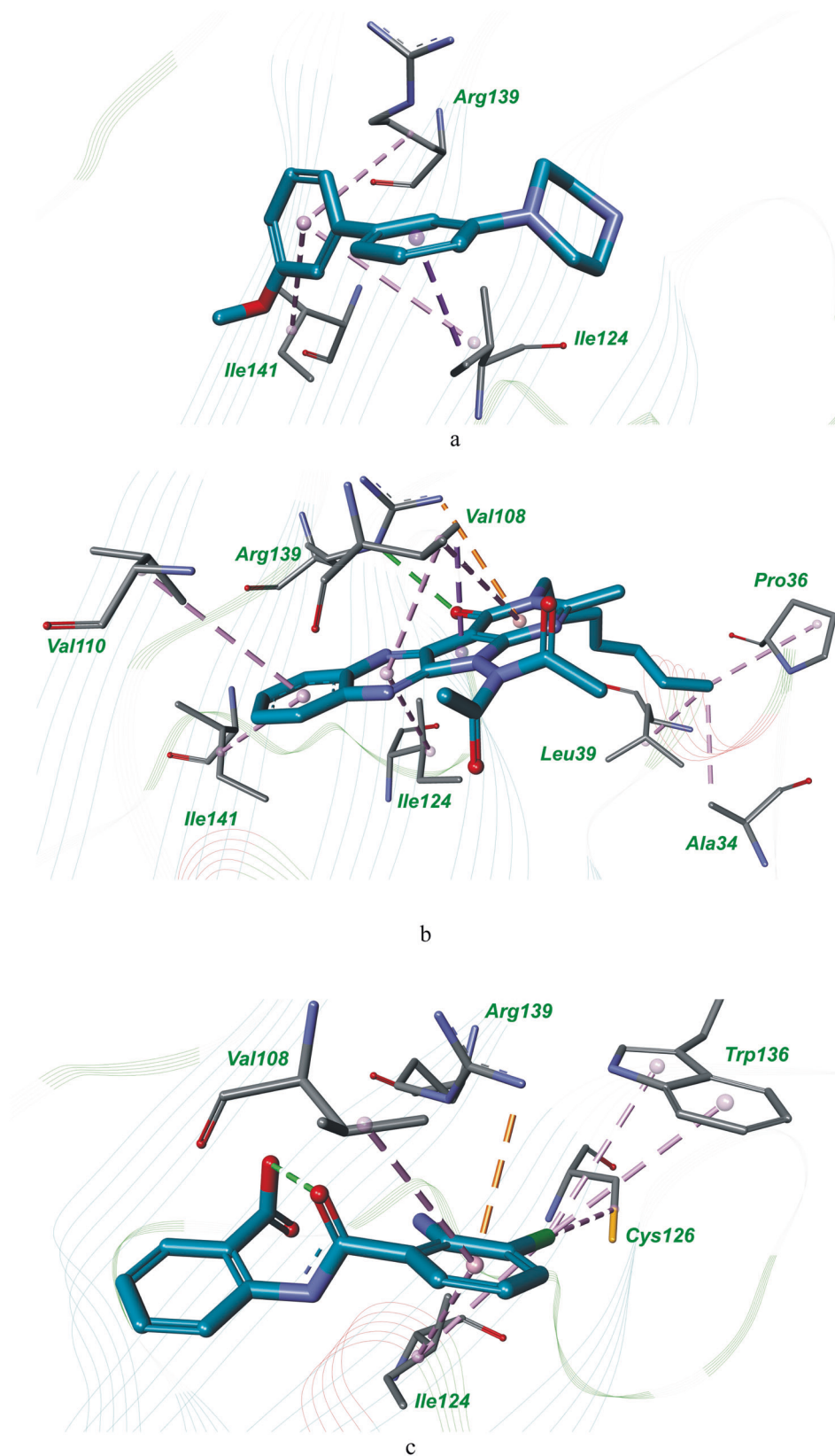
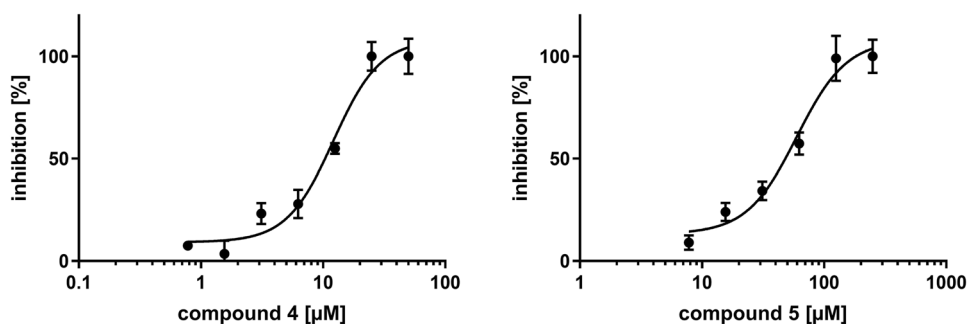**Fig. 4** Determination of IC$_{50}$ values for compounds **4** and **5**

Table 1 Selectivity results from screening of compounds **4** and **5** against various cysteine proteases

Inhibition	sortase A	hCatL	hCatB	rhodesain	SARS-CoV2 M^{pro}
Compound **4** (25 μM)	100%	2.3%	11.8%	37.3%	36.2%
Compound **5** (125 μM)	99%	7.6%	7.1%	10.9%	16.5%

Fig. 5 Determination of the K$_D$ value for compound **5** by MST. The normalized thermophoresis time traces (**a**) display significant bumps and a pronounced shift with higher concentrations of **5**. The sigmoidal fit of response-concentration blot after 10 s laser-on time (**b**) determined the K$_D$ of **5** to be 189 μM
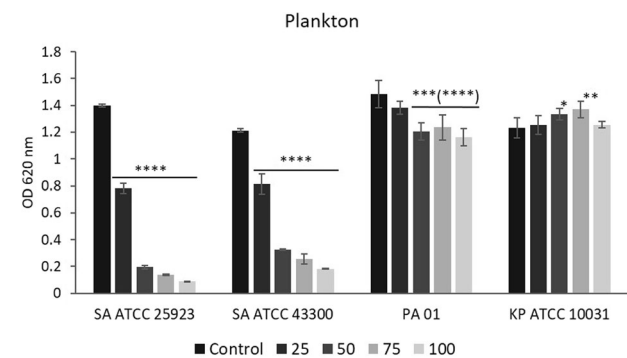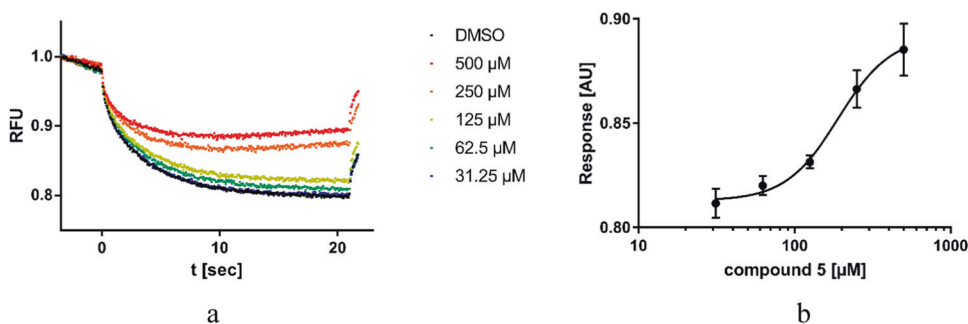

a

b

Fig. 6 The level of planktonic bacteria biomass after treatment with compound **5**. The level of planktonic biomass of S. *aureus* (SA) ATCC 25923 (MS), S. *aureus* (SA) ATCC 43300 (MR), *P. aeruginosa* (PA) PA 01, *K. pneumoniae* (KP) ATCC 10031 formed in the presence of compound **5** in a concentration of 25, 50, 75, 100 mg l^{-1} (which corresponds to 86 μM, 172 μM, 258 μM, 344 μM) or without (control) following 24 h of incubation measured as the optical density at 620 nm. Statistical significance compared to control. *$p < 0.05$, **$p < 0.01$, ***$p < 0.005$, ****$p < 0.001$

Statistical analysis

Replicate data were processed using the statistical software package OriginPro 7.0 and MS Excel for Windows. All results are presented as the mean ± standard deviation. A value of $p < 0.05$ was considered statistically significant.

Results and discussion

In order to identify novel inhibitors of *S. aureus* sortase A the molecular docking and pharmacophore screening of the OTAVA compound collection [32] containing about 250,000 compounds were performed. There were 96 compounds selected for in vitro assays following the results of virtual screenings including 39 compounds selected according to the docking assay and 57 compounds selected in the pharmacophore screening assay.

First, the 96 test compounds were screened for inhibition of sortase A in a Förster resonance energy transfer (FRET)-based enzyme assay using Abz-LPETG-Dap(dnp)-OH as a substrate. For this purpose, an initial inhibitor concentration of 200 μM was chosen in order to identify weaker inhibitors also. The inhibition data (triplicates) for all 96 compounds are available as supplementary material (Table S1). Of the 96 compounds, 17 showed inhibition of >50% at 200 μM and were chosen for further characterization. There were a number of visibly colored compounds that could potentially interfere in the FRET-based enzyme assay. The potential

quenching of the FRET-fluorophore (anthranilic acid) was determined by measuring the fluorescence of variable concentrations of anthranilic acid (1.25–10 μM) with 200 μM of each inhibitory compound. The inhibition caused by this quenching of the fluorophore was subtracted from the inhibition in the sortase A enzyme assay. As seen in Table S1, 12 of the 17 primarily identified hits were actually false-positives. However, 5 out of 96 compounds showed >50% corrected inhibition at 200 μM. The chemical structures of these compounds are shown in Fig. 1.

The compounds 1 and 2 were found with pharmacophore screening toward pharmacophore models generated based on the crystal structure of *S. aureus* sortase A with PDB accession code 2MLM [26]. The mapping of compounds 1 and 2 on corresponding pharmacophore models is shown in Fig. 2.

The compounds 3, 4, and 5 were identified according to molecular docking results. The complexes of these compounds with amino acid residues in the active site of *S. aureus* sortase A are presented in Fig. 3.

According to FRET analysis data, two compounds 4 and 5 demonstrated strong inhibition of > 95%. Concentration-dependent inhibition series of these two compounds were performed to calculate the IC_{50} values. The IC_{50} values for compounds 4 and 5 were determined to be 12.1 μM and

59.7 μM, respectively (Fig. 4). For the other compounds, the inhibition at 200 μM was too low to determine an IC_{50} value and testing at higher concentrations was limited by solubility.

In order to show whether the inhibition is specific for sortase A, these two compounds were tested on four additional cysteine proteases. This selectivity measurement was performed against human cathepsin L (hCatL), cathepsin B (hCatB), the cathepsin L-like parasite protease rhodesain, and the severe acute respiratory syndrome coronavirus 2 main protease (SARS-CoV2M^{pro}) at an inhibitor concentration of 25 μM for compound 4 and 125 μM for compound 5. Only slight inhibition beyond the sortase A target was found for the two inhibitors indicating selective inhibition (Table 1).

As an orthogonal assay strategy, microscale thermophoresis (MST) experiments were performed with the identified hit compounds at 500 μM inhibitor concentration (Fig. 5). A change in the thermophoresis curves in the presence of inhibitors suggests selective binding of the compounds to sortase A. For compound 5, the thermophoresis response changed significantly. For the other compounds, no thermophoresis changes were observed, which is either because (1) these substances do not bind selectively to sortase A or (2) the binding does not lead to a sufficient change of the hydration
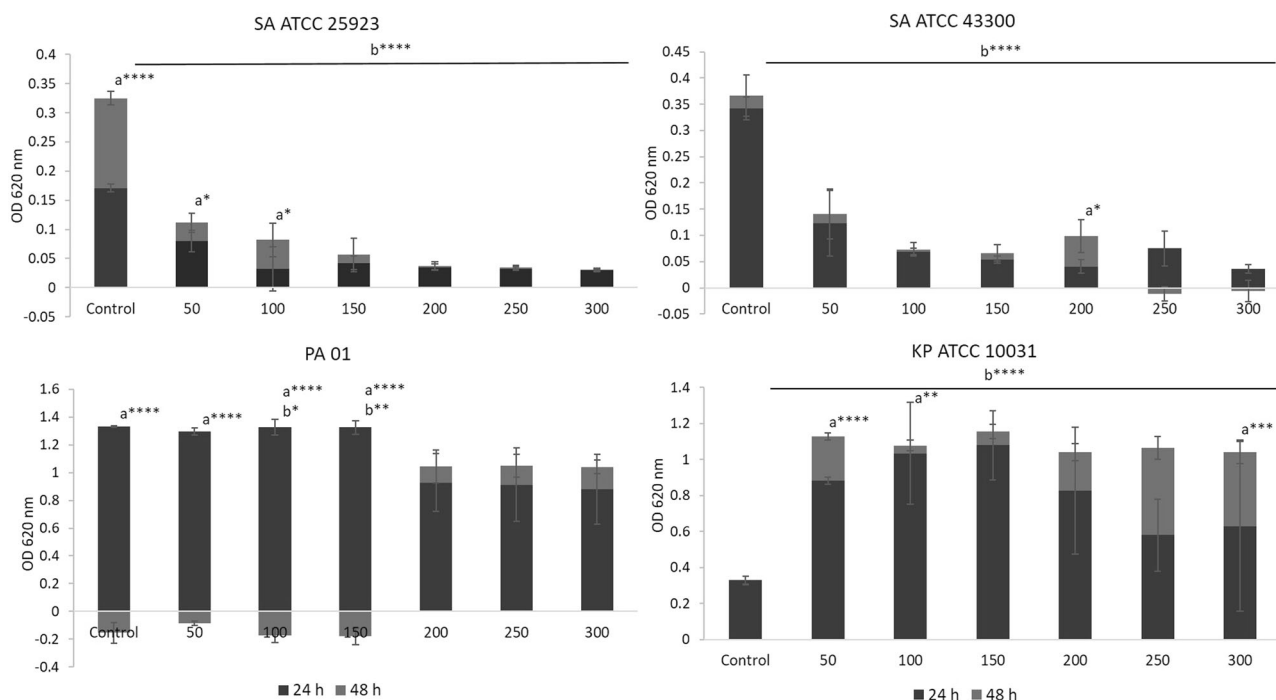

Fig. 7 The level of the total bacteria biofilm biomass after treatment with compound 5. The level of total biofilm biomass of S. *aureus* (SA) ATCC 25923 (MS), S. *aureus* (SA) ATCC 43300 (MR), *P. aeruginosa* (PA) PA 01, *K. pneumoniae* (KP) ATCC 10031 formed in the presence of compound 5 in concentrations of 50, 100, 150, 200, 250, 300 mg l^{-1} (which corresponds to 172 μM, 344 μM, 516 μM, 688 μM,

860 μM, 1032 μM) or without (control) following the first day (dark grey, 24 h) and the second day (light grey, 48 h) of incubation measured as the optical density at 620 nm. a statistical significant differences of the second-day growth compared to the first day of incubation; b statistically significant difference compared to control. * $p < 0.05$, ** $p < 0.01$, *** $p < 0.005$, **** $p < 0.001$
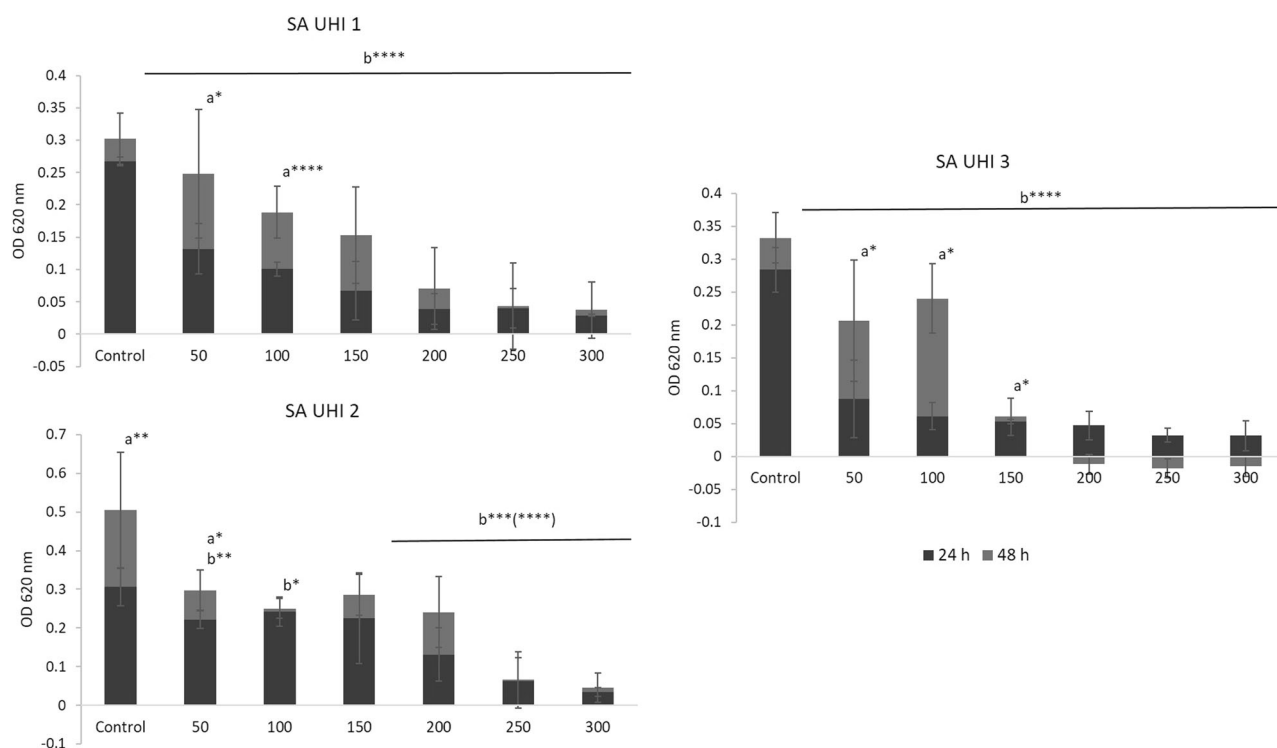
Fig. 8 The level of the total biofilm biomass of *S. aureus* strains after treatment with compound **5**. The level of the total biofilm biomass of three *S. aureus* wild type UHI strains formed in the presence of compound **5** in a concentration of 50, 100, 150, 200, 250, 300 mg l^{-1} (which corresponds to 172 μM, 344 μM, 516 μM, 688 μM, 860 μM, 1032 μM) or without (control) following the first day (dark grey, 24 h) and the second day (light grey, 48 h) of incubation measured as the optical density at 620 nm. a statistical significance of the second-day growth compared to the first day of incubation; b statistical significance compared to control. *$p < 0.05$, **$p < 0.01$, ***$p < 0.005$, ****$p < 0.001$
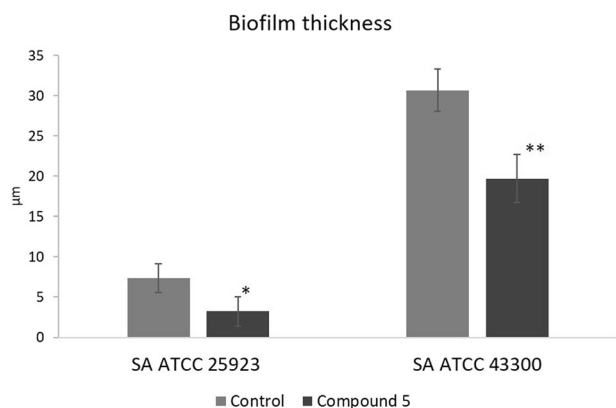

Fig. 9 The thickness of *S. aureus* biofilms. The average thickness of the two-day-old biofilms produced by two S. aureus strains ATCC 25923 and ATCC 43300 was observed by confocal laser scanning microscopy (CLSM). Statistical significance of compared to control. *$p < 0.05$, **$p < 0.01$

shell, or (3) the inhibitor concentrations are too low compared to the affinity. MST is also a sensitive method to identify ligand-induced protein aggregation, as expressed by bumpy thermophoresis curves. The thermophoresis curves demonstrated that compound **4** is likely to be an aggregator. The identified binder compound **5** was subsequently analyzed in a

1:1 dilution series, beginning with 500 μM by MST to determine the K$_D$ value. For compound **5**, a K$_D$ value of 189 μM was found (Fig. 5).

To investigate if any of the other hit structures is likely to cause assay-interfering aggregation, all hit compounds were subjected to a turbidimetry screening. The optical density (OD$_{610}$) was measured over time (assay buffer, 200 μM compound concentration). The optical density did increase over time for compound **4**, indicating that this substance can form microscopic aggregates in a protein-independent manner due to its high hydrophobicity. The other four hit compounds did not cause precipitation detectable by turbidimetry. These findings are in line with our MST measurements, indicating the formation of aggregates at higher concentrations of **4**.

The effects of the hit compound **5** against *S. aureus* free-living plankton and sessile attached biofilm-forming bacterial cultures were determined. The direct antibacterial effect of the compound **5** and its specificity against free-living bacteria were studied using four typical strains, specifically, methicillin-sensitive (MS) *S. aureus* ATCC 25923, methicillin-resistant (MR) *S. aureus* ATCC 43300, *Pseudomonas aeruginosa* PA 01, and *Klebsiella pneumoniae* ATCC

10031. Four concentrations, particularly, 25, 50, 75, and 100 mg l^{-1} of compound **5** were used to evaluate antibacterial effect against planktonic culture. The compound showed statistically significant reduction in plankton growth for both *S. aureus* strains for all the concentrations used. The lowest concentration of 25 mg l^{-1} reduced the population of *S. aureus* ATCC 25923 and *S. aureus* ATCC 43300 by 42% and 33%, respectively (Fig. 6). The rest of the concentration demonstrated 7- and 4-fold growth reduction for *S. aureus* ATCC 25923 and *S. aureus* ATCC 43300. Interestingly, there was no substantial effect of the compound onto *P. aeruginosa* PA 01: only 20% growth decrease was observed for 50, 75, and 100 mg l^{-1}. It was also noticed that compound **5** showed stimulative activity for *K. pneumoniae* ATCC 10031, increasing the growth by 14–16% whereas exposure to 50 and 75 mg l^{-1} had no effects. This suggests specificity of compound **5** for the target, associated with free-living *S. aureus* cells.

Bacteria colonize the econiche through biofilm formation which is the dominant form of bacterial persistence [36].
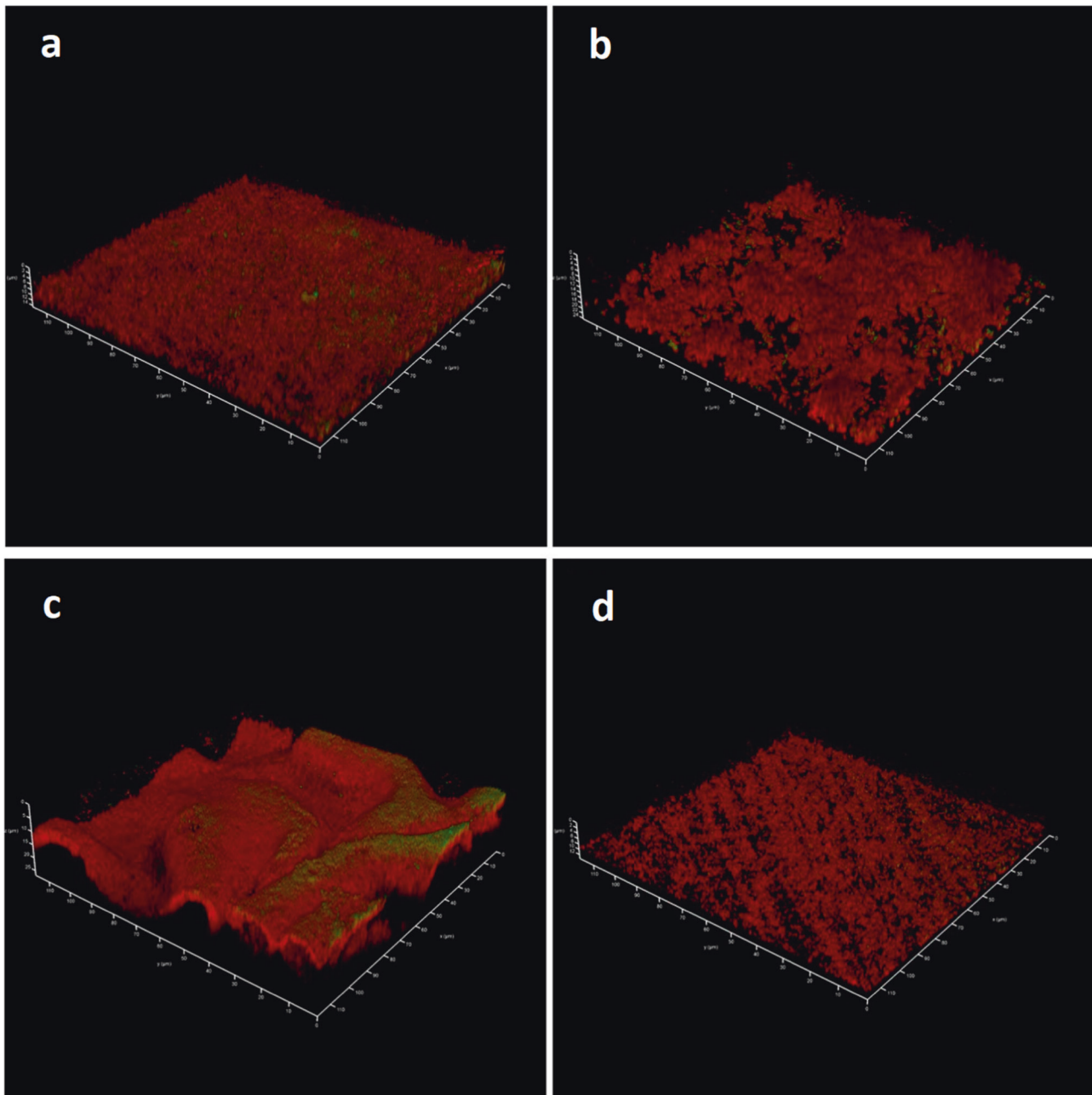

Fig. 10 Biofilm structure of *S. aureus* strains. Biofilm structure of two S. *aureus* strains, ATCC 25923 (**a**, **b**) and ATCC 43300 (**c**, **d**) following 2 days of incubation in the presence of compound **5** in a concentration of 100 mg l^{-1} (**b**, **d**) or without (**a**, **c**). Staining was performed with ethidium bromide to visualize cells and AmyGreen to visualize amyloids, CLSM

The bacterial strains used in the planktonic assay are well-known biofilm producers [37]. The biofilm formation by these four strains was measured at 24 and 48 h of incubation in presence of compound **5** in varying concentrations (50, 100, 150, 200, 250, and 300 mg l^{-1}) to observe the dynamic change in the biofilm biomass. Increase in biofilm mass was measured as difference between 24- and 48-hour biofilm biomass, measured spectrophotometrically (Fig. 7). In this biofilm formation assay, the high specificity of compound **5** for the *S. aureus*-associated target was also confirmed since all tested concentrations effectively reduced or suppressed biofilm formation in *S. aureus*. On the contrary, compound **5** did not suppress *P. aeruginosa* PA 01 biofilms and, as before, showed stimulative activity on *K. pneumoniae* ATCC 10031 stationary culture, resulting in a 4-fold increase in biofilm formation. This might be explained by differences in the surface proteins onto the outer surface of *K. pneumoniae* cells, since sortase A is a transpeptidase enzyme that is responsible for tagging many surface-associated proteins. This, in turn, might inhibit some regulatory or metabolic pathways associated with biofilm formation and disruption in *K. pneumoniae*. Indeed, we found that class A sortase (SrtA) in *K. pneumonia* beares a high homology to SrtA of *S. aureus* with an amino-acid sequence identity of 40.5%. However, there are no available data on how SrtA suppression might affect *K. pneumoniae* biofilm. We hypothesized that there might be some stimulation of the biofilm formation by *K. pneumoniae* when SrtA is repressed by an unknown mechanism.

Since biofilm formation is exacerbates bacterial infection, we wondered how pathogenic wild type *S. aureus* isolates might respond to compound **5**. To study this, three isolates from Ukrainian hospital (UHI1-3) were obtained. These isolates had extended antibiotic resistances (Table S2), which were characterized according to EUCAST (European Committee on Antimicrobial Susceptibility Testing) recommendations [35], and were used to screen for antibiofilm activity of compound **5** (Fig. 8).

It was shown that the UHI were less sensitive than the ATCC strains to compound **5**, in general, with the biofilm inhibitory activity starting from 50 mg l^{-1} as before.

It was recently shown that SrtA inhibition may be associated with biofilm suppression in *Streptococcus mutans*, *Streptococcus pneumoniae*, and *S. aureus* [38–42]. Thus, we wondered how compound **5** could influence biofilm development. For this, we measured the average thickness of the biofilms, developed by *S.aureus* ATCC strains in the presence of 100 mg l^{-1} (344 μM) of compound **5** or without (Fig. 9). We noticed that the thickness of the biofilms was reduced by compound **5** in both strains.

We also investigated the structure of biofilms produced by two ATCC strains in the presence of the studied compound (Fig. 10). As seen in the microscopy image, the
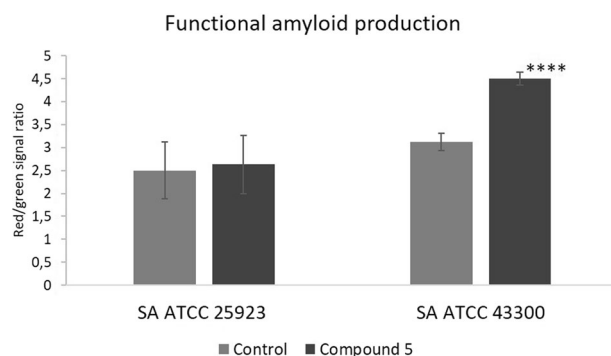

Fig. 11 The cell/amyloid biomass ratio calculated from total pixels in 3D. The cell/amyloid biomass ratio calculated from total pixels in CLSM imaging of 48 h old *S.aureus* (SA) ATCC 25923 and *S. aureus* (SA) ATCC 43300 biofilms, formed in the presence of 100 mg/L (344 μM) of compound **5** or without (control). Statistical significance compared to control. ****$p < 0.001$

spatial structure was substantially affected by the presence of the compound.

In order to evaluate how compound **5** influenced functional amyloid production of both *S. aureus* strains, we calculated the ratio of the total amount of red and green pixels in the 3D imaging obtained with CLSM above. Here, the red signal corresponded to the total cell biomass amount, following ethidium bromide staining whereas the green signal, produced by the newly introduced amyloid-specific stain, specifically visualized bacterial functional amyloid fibers as we described before [37]. The ratio shows that there was no effect of compound **5** on amyloid production by the weaker biofilm-forming strain ATCC 25923 (Fig. 10a) whereas the other strain ATCC 43300, which produced stronger biofilm (Fig. 10c), demonstrated a reduction in amyloid production (Fig. 11).

Conclusions

Using a molecular docking approach, we identified the *S. aureus* sortase A inhibitor 2-(2-amino-3-chloro-benzoylamino)-benzoic acid (**5**), possessing an IC$_{50}$ value of 59.7 μM. This compound is selective towards SrtA, compared to other four cysteine proteases–CatL, CatB, rhodesain and the SARS-CoV2 M^{pro}. Also, this compound demonstrates *S. aureus*–specific antibacterial and anti-biofilm effects by reducing planktonic cells and biofilm thickness. Compound **5** shows good specificity since it does not reduce *P. aeruginosa* and stimulates *K. pneumoniae* biofilms. This suggests that all potential SrtA inhibitors should be tested against Gram-negative bacteria due to the possibility of a stimulative effect.

Therefore, compound **5** can be a valuable candidate for further chemical optimization and biological research.

Compliance with ethical standards

Conflict of interest The authors declare no competing interests.

Publisher's note Springer Nature remains neutral with regard to jurisdictional claims in published maps and institutional affiliations.

References

1. Ericson JE, Popoola VO, Smith PB, Benjamin DK, Fowler VG, Benjamin DK JR, et al. Burden of invasive *Staphylococcus aureus* infections in hospitalized infants. JAMA Pediatr. 2015;169:1105–11.
2. Defres S, Marwick C, Nathwani D. MRSA as a cause of lung infection including airway infection, community-acquired pneumonia and hospital-acquired pneumonia. Eur Respir J. 2009;34:1470–6.
3. Ippolito G, Leone S, Lauria FN, Nicastri E, Wenzel RP. Methicillin-resistant *Staphylococcus aureus*: the superbug. Int J Infect Dis. 2010;14:S7–S11.
4. Gardete S, Alexander, Tomasz A. Mechanisms of vancomycin resistance in *Staphylococcus aureus*. J Clin Invest. 2014;124: 2836–40.
5. Kali A. Antibiotics and bioactive natural products in treatment of methicillin-resistant *Staphylococcus aureus* (MRSA): a brief review. Pharmacogn Rev. 2015;9:29–34.
6. Kaur DC, Chate SS. Study of antibiotic resistance pattern in methicillin-resistant *Staphylococcus aureus* with special reference to newer antibiotic. J Glob Infect Dis. 2015;7:78–84.
7. Arunkumar V, Prabagaravarthanan R, Bhaskar M. Prevalence of methicillin-resistant *Staphylococcus aureus* (MRSA) infections among patients admitted in critical care units in a tertiary care hospital. Int J Res Med Sci. 2017;5:2362–6.
8. McGuinness WA, Malachowa N, DeLeo FR. Vancomycin resistance in *Staphylococcus aureus*. Yale J Biol Med. 2017;90:269–81.
9. Mazmanian SK, Liu G, Ton-That H, Schneewind O. *Staphylococcus aureus* sortase, an enzyme that anchors surface proteins to the cell wall. Science 1999;285:760–3.
10. Zhang J, Liu H, Zhu K, Gong S, Dramsi S, Wang YT, et al. Anti-infective therapy with a small molecule inhibitor of *Staphylococcus aureus* sortase. Proc Natl Acad Sci USA. 2014;111:13517–22.
11. Cascioferro S, Totsika M, Schillaci D. Sortase A: an ideal target for anti-virulence drug development. Micro Pathog. 2014;77: 105–12.
12. Barthels F, Marincola G, Marciniak T, Konhäuser M, Hammerschmidt S, Bierlmeier J, et al. Asymmetric disulfanylbenzamides as irreversible and selective inhibitors of *Staphylococcus aureus* sortase A. ChemMedChem 2020;15:839–50.
13. Spirig T, Weiner EM, Clubb RT. Sortase enzymes in gram-positive bacteria. Mol Microbiol. 2011;82:1044–59.
14. Marraffini LA, Dedent AC, Schneewind O. Sortases and the art of anchoring proteins to the envelopes of gram-positive bacteria. Microbiol Mol Biol Rev. 2006;70:192–221.
15. Cascioferro S, Totsika M, Schillaci D. Sortase A an ideal target for anti-virulence drug development. Micro Pathog. 2014;77:105–12.
16. Cascioferro S, Raffa D, Maggio B, Raimondi MV, Schillaci D, Daidone G. Sortase A inhibitors: recent advances and future perspectives. J Med Chem. 2015;58:9108–23.
17. Guo Y, Cai S, Gu G, Guo Z, Long Z. Recent progress in the development of sortase A inhibitors as novel anti-bacterial virulence agents. RSC Adv. 2015;5:49880–9.
18. Ha MW, Yi SW, Paek SM. Design and synthesis of small molecules as potent *Staphylococcus aureus* sortase A inhibitors. Antibiotics 2020;9:706.
19. Alharthi S, Alavi SE, Moyle PM, Ziora ZM. Sortase A (SrtA) inhibitors as an alternative treatment for superbug infections. Drug Disco Today. 2021;26:2164–72.
20. Nitulescu G, Margina D, Zanfirescu A, Olaru OT, Nitulescu GM. Targeting bacterial sortases in search of anti-virulence therapies with low risk of resistance development. Pharmaceuticals 2021;14:415.
21. Volynets G, Vyshniakova H, Nitulescu G, Nitulescu GM, Ungurianu A, Margina D, et al. Identification of novel antistaphylococcal hit compounds targeting sortase A. Molecules 2021;26:7095.
22. Bodian DL, Yamasaki RB, Buswell RL, Stearns JF, White JM, Kuntz ID. Inhibition of the fusion-inducing conformational change of influenza hemagglutinin by benzoquinones and hydroquinones. Biochemistry 1993;32:2967–78.
23. Ewing TJ, Makino S, Skillman AG, Kuntz ID. DOCK 4.0: search strategies for automated molecular docking of flexible molecule databases. J Comput-Aided Mol Des. 2001;15:411–28.
24. Ring CS, Sun E, McKerrow JH, Lee GK, Rosenthal PJ, Kuntz ID, et al. Structure-based inhibitor design by using protein models for the development of antiparasitic agents. Proc Natl Acad Sci USA. 1993;90:3583–7.
25. Stoichet BK, Stroud RM, Santi DV, Kuntz ID, Perry KM. Structure-based discovery of inhibitors of thymidylate synthase. Science 1993;259:1445–50.
26. Zhulenkovs D, Rudevica Z, Jaudzems K, Turks M, Leonchiks A. Discovery and structure-activity relationship studies of irreversible benzisothiazolinone-based inhibitors against *Staphylococcus aureus* sortase A transpeptidase. Bioorg Med Chem. 2014;22:5988–6003.
27. Yakovenko OY, Oliferenko A, Golub A, Bdzhola V, Yarmoluk S. The new method of distribution integrals evaluations for high throughput virtual screening. Ukr Bioorg Acta. 2007;1:52–62.
28. Yakovenko O, Oliferenko AA, Bdzhola VG, Palyulin VA, Zefirov NS. Kirchhoff atomic charges fitted to multipole moments: implementation for a virtual scrrening system. J Comput Chem. 2008;29:1332–43.
29. Kovalenko OP, Volynets GP, Rybak MY, Starosyla SA, Gudzera OI, Lukashov SS, et al. Dual-target inhibitors of mycobacterial aminoacyl-tRNA synthetases among N-benzylidene-N'-thiazol-2-yl-hydrazines. Medchemcomm 2019;10:2161–9.
30. Discovery Studio Visualizer 4.0. https://www.3dsbiovia.com/products/collaborative-science/biovia-discovery-studio/visualization-download.php, (accessed May 2019).
31. Suree N, Liew CK, Villareal VA, Thieu W, Fadeev EA, Clemens JJ, et al. The structure of the *Staphylococcus aureus* sortase-substrate complex reveals how the universally conserved LPXTG sorting signal is recognized. J Biol Chem. 2009;284:24465–77.
32. We used a database of commercially available compounds (Otava Ltd., http://www.otavachemicals.com/).
33. Schmohl L, Bierlmeier J, von Kügelgen N, Kurz L, Reis P, Barthels F, et al. Identification of sortase substrates by specificity profiling. Bioorg Med Chem 2017;25:5002–7.
34. Klein P, Barthels F, Johe P, Wagner A, Tenzer S, Distler U, et al. Naphthoquinones as covalent reversible inhibitors of cysteine proteases – studies on inhibition mechanism and kinetics. Molecules 2020;252:064.
35. EUCAST guidelines for detection of resistance mechanisms and specific resistances of clinical and/or epidemiological importance, Version 1.0, December Effect of Combination l-Citrulline and Metformin Treatment on Motor Function in Patients With Duchenne Muscular Dystrophy: A Randomized Clinical Trial, JAMA network open, 2013, 2, 1914171.
36. Moshynets OV, Spiers AJ. Viewing biofilms within the larger context of bacterial aggregations. In Biofilms: InTech Press; 2016. p. 3-22.

37. Moshynets O, Chernii S, Chernii V, Losytskyy M, Karakhim S, Czerwieniec R, et al. Fluorescent β-ketoenole AmyGreen dye for visualization of amyloid components of bacterial biofilms. Methods Appl Fluoresc. 2020;8:035006.

38. Hu P, Huang P, Chen MW. Curcumin reduces *Streptococcus mutans* biofilm formation by inhibiting sortase A activity. Arch Oral Biol. 2013;58:1343–8.

39. Huang P, Hu P, Zhou SY, Li Q, Chen WM. Morin inhibits sortase A and subsequent biofilm formation in *Streptococcus mutans*. Curr Microbiol. 2014;68:47–52.

40. Wang J, Song M, Pan J, Shen X, Liu W, Zhang X, et al. Quercetin impairs *Streptococcus pneumonia* biofilm formation by inhibiting sortase A activity. J Cell Mol Med. 2018;22:6228–37.

41. Thappeta KRV, Zhao LN, Nge CE, Crasta S, Leong CY, Ng V, et al. In-silico identified new natural sortase A inhibitors disrupt *S. aureus* biofilm formation. Int J Mol Sci. 2020;21:8601.

42. Wang L, Wang G, Qu H, Wang K, Jing S, Guan S, et al. Taxifolin, an inhibitor of sortase A, interferes with the adhesion of methicillin-resistant *Staphylococcal aureus*. Front Microbiol. 2021;12:686864.